Results in Physics 62 (2024) 107806

Contents lists available at ScienceDirect

Results in Physics

journal homepage: www.elsevier.com/locate/rinp

Machine learning assisted high-precision temperature sensor in a multimode microcavity

Rui Song [a,b,1], Xuan Zhang [b,1], Shuang Feng [c], Songyi Liu [a,b], Bing Duan [a,b,*], Daquan Yang [a,b,**]

[a] State Key Laboratory of Information Photonics and Optical Communications, Beijing University of Posts and Telecommunications, Beijing 100876, China
[b] School of Information and Communication Engineering, Beijing University of Posts and Telecommunications, Beijing 100876, China
[c] School of the Future, Beijing University of Posts and Telecommunications, Beijing 100876, China

ARTICLE INFO

Keywords:
WGM microcavity
Multimode sensing
Temperature sensor
Machine Learning

ABSTRACT

Whispering gallery mode (WGM) microcavities are excellent platforms for ultra-sensitive sensing due to high-quality factor and small mode volume. However, the conventional sensing method by tracking single-mode changes is difficult to fully utilize the sensing information, which limits the measurement precision and dynamical range. Here, we demonstrate a high-precision temperature sensor based on the multimode sensing method in a packaged microbubble resonator (PMBR). Remarkably, a low-cost broadband spectrum source is used as probe light to provide more sensing modes for high-precision measurement. Empowered by a machine learning method, the multimode spectral information are fully utilized, and the true temperature is precisely readout with mean-squared error (MSE) of 0.0138. The detection limit is lower three times than single-mode sensing method, capable of reaching 0.117 °C. In addition, the correlation coefficient (R^2) between predictions and truth is as high as 0.9996 within the measurement range of 25–45 °C. With the low-cost laser source and high detection precision, this work provides a new perspective for intelligent optical microcavity sensors and their engineering applications.

Introduction

Whispering gallery mode (WGM) microcavities [1–3] with enhanced light-matter interaction have attracted extensive research interest in ultrasensitive sensors, low-threshold lasers, quantum optical devices, and optical frequency combs [4–8]. Particularly, in highly sensitive optical sensing, WGM microcavities have reached the level of single-molecule and single-ion detection by combining surface plasmon, optical spring effect, photoelectric heterodyne and laser mode-locking [9]. With high sensitivity and fast response, they are also widely used in the measurement of physical parameters, such as temperature, pressure, and magnetic field [10–12]. All of the above WGM sensors are implemented by tracking single mode changes, such as mode shifts, splitting and linewidth broadening [4,13,14]. However, this conventional single-mode tracking method ignores and wastes the sensing information from other resonances, constraining the detection precision. On the other hand, the dynamic measurement range is limited by the laser source, which is mainly because the single-mode method usually does not work when the tracking mode removes out the laser scanning range. Although the dynamic measurement range can be improved by increasing the laser sweep range, which results in a degradation of the resolution due to the limited number of data points per spectrum. In addition, the single-mode WGM sensors measure the relative changes, and thus the actual value is difficult to readout directly without baseline and calibration.

Fortunately, there are multiple modes in WGM microcavity, exhibiting different responses to the target parameters. Therefore, the measurement uncertainty can be effectively reduced by fusing the sensing information carried by these resonant modes [15–17]. So far, several works have been reported for high-precision detection based on the multimode sensing method [18–22]. For example, Liao et al. demonstrate an optical WGM barcode sensing method based on multiple resonant modes, achieving the direct readout of actual temperature [19]. In the specific implementation, the WGM spectrums at different temperatures are transformed as barcodes to establish the database. Subsequently, the most similar barcode is retrieved by comparing the barcode from a particular measurement with the standard barcode in the databases. Finally, the actual temperature is determined based on the collective shift between the two barcodes. The detection accuracy of this method relies on the database size, and

* Corresponding author.
** Corresponding author at: School of Information and Communication Engineering, Beijing University of Posts and Telecommunications, Beijing 100876, China.
E-mail addresses: duanbing@bupt.edu.cn (B. Duan), ydq@bupt.edu.cn (D. Yang).
[1] These authors contributed equally to this work.

https://doi.org/10.1016/j.rinp.2024.107806
Received 10 April 2024; Received in revised form 13 May 2024; Accepted 2 June 2024
Available online 4 June 2024

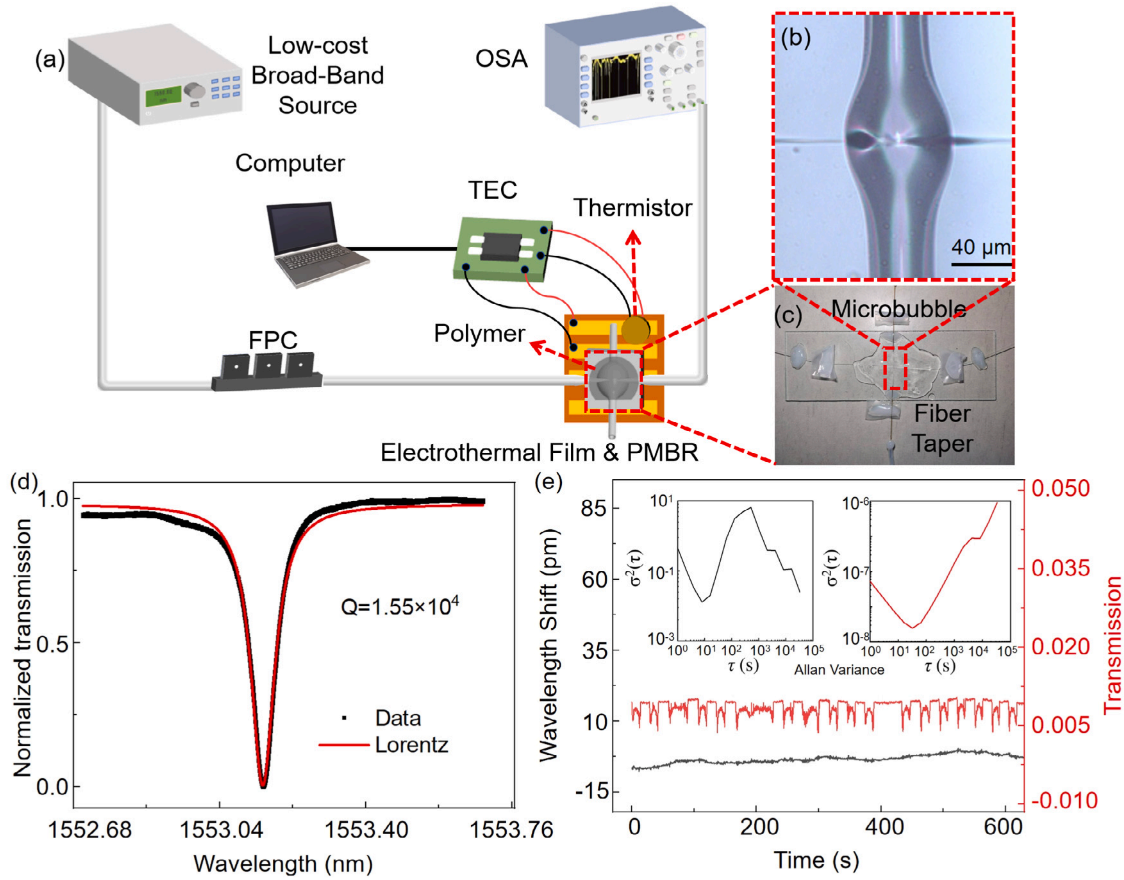

Fig. 1. (a) Experimental setup for temperature sensing bases on broadband laser source. OSA: optical spectrum analyzer, TEC: thermoelectric cooler, FPC: fiber polarization controller, PMBR: packaged microbubble resonator. (b) Microscope image of PMBR with a diameter of about 80 μm. (c) Physical image of the PMBR. (d) Transmission spectra of PMBR near 1553 nm. The *Q*-factor of 1.55×10^4 is obtained via Lorentzian fitting. (e) Long-term stability of wavelength shift (black) and transmission (red) of PMBR. Inset: Allan variance of wavelength shift (left) and transmittance (right).

the collection of major databases is time- and resource-consuming. Moreover, the multimode sensing methods have been widely used in multiple parameters sensing, such as the simultaneous measurement of temperature and stress, concentration and humidity, temperature and pressure, and mixed gas [20,23–25]. In the multi-parameter sensing, sensing matrix is a commonly used method for data process, which is only applicable when the sensing mode and target parameter are in a linear relationship. Therefore, there is a need to find a general, time- and effort-saving data processing method for multimode sensing methods. Machine learning with powerful data-processing capacity and nonlinear modeling capability is considered an alternative approach to extract sensing information from multi-mode spectra [26,27]. It has been widely used in optical sensing signal process, exhibiting a higher performance compared with other sensing schemes [28–31]. For example, machine learning have been used in tumour diagnosis and classification based on Raman spectroscopy and Raman imaging, effectively improving the accuracy of diagnosis [29]. Recently, several machine learning algorithms such as Generalized Regression Neural Network (GRNN), Multi-Layer Perceptron (MLP), and Artificial Neural Network (ANN), have been employed in the multimode sensing methods based on optical microcavity, enabling the high precision measurement of temperature, and pressure, as well as identification of concentration and species of solution mixtures [15,32,33]. However, the multimode sensing method based on machine learning usually requires a wide sweep frequency range to increase the number of sensing modes to achieve high detection precision [34]. These tunable lasers are expensive and bulky, commonly requiring an optical bench and a separate laser controller, making WGM microcavity sensors difficult to take out of the lab and impeding the practicability and engineering.

In this work, based on a low-cost broadband laser source, we demonstrate a machine learning-assisted high-precision temperature sensor in a packaged microbubble resonator (PMBR). By fusing these sensing modes using machine learning, smaller detection uncertainty can be achieved. Here, a three layer perceptron neural network is employed to retrieve the actual temperature. When the temperature changes from 25 °C to 45 °C in the step of 0.5 °C, the corresponding transmission spectra are experimentally captured as a dataset to train and test the network model. The true temperatures are precisely readout with a mean-squared error (MSE) of 0.0138 within the measurement range of 25–45 °C. and the correlation coefficient (R^2) of 0.9996 is realized. The detection limit of 0.117 °C is achieved, which is a quarter of the single-mode sensing method. This work exhibits the potential of the low-cost broadband laser source in multimode microcavity sensors. Meanwhile, the cross-application with machine learning further improves the detection precision, laying the foundation for optical intelligent sensors and their engineering applications.

Fabrication and characterization

The experimental setup is illustrated in Fig. 1(a). An oblate geometry microbubble resonator (MBR) is chosen due to the dense spectrum, which is more suitable for the multimode sensing method. MBR is fabricated using silica capillaries via the thermal expansion method [35,36]. The whole fabrication process involves three steps. Firstly, the capillary is heated with a hydrogen flame and stretched to a tapered waist diameter of about 30 μm. Subsequently, one end of the capillary is sealed with ultraviolet (UV) glue, and another is connected to a syringe for pressurization. Finally, the two counter-propagating beams from a

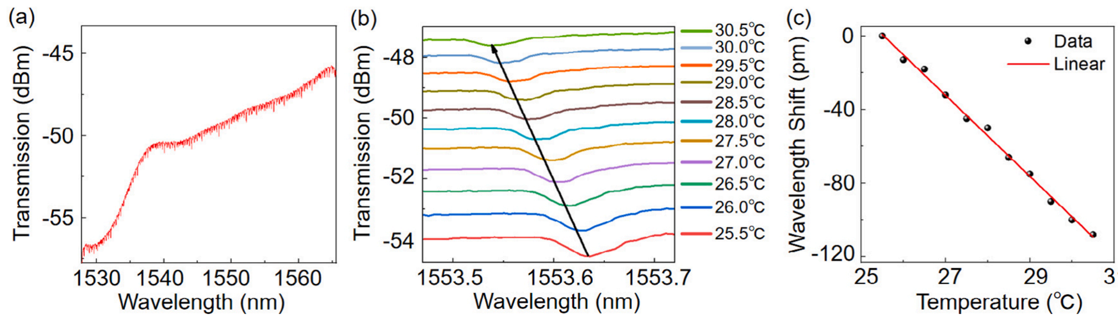

Fig. 2. (a) Experimentally measured transmission spectra of the microcavity under the excitation of a broad-spectrum laser source at 26 °C. (b) Tracking detection using the resonant modes shown by the arrows when the temperature was increased from 25.5 to 30.5 °C. (c) Mode shift versus temperature change.

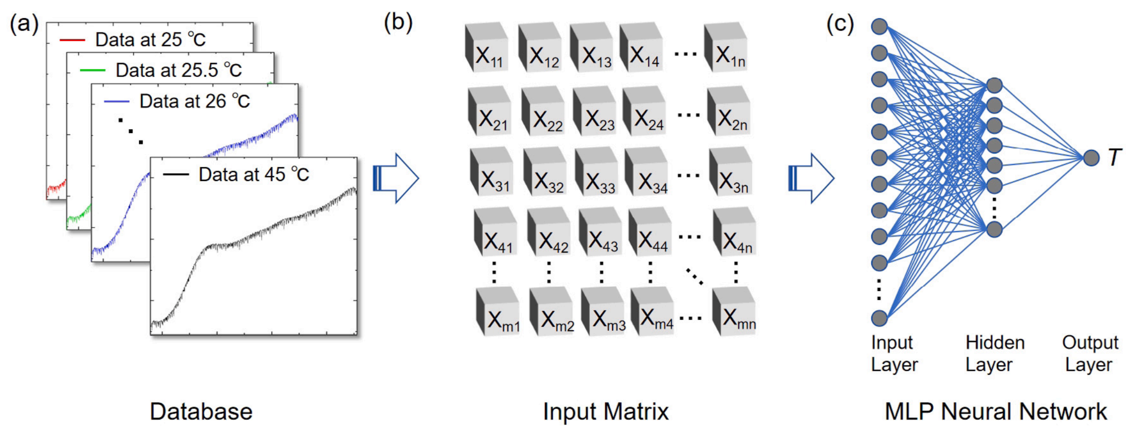

Fig. 3. The transmission spectra are collected to build a database (a), and then converted into a matrix (b), where m is the number of samples and n is the number of data points of the samples. (c) Schematic diagram of the MLP neural network.

CO_2 laser heat the pressurized area, and the capillary gradually expands into a bubble, as shown in Fig. 1(b). In the measurement experiment, a low-cost broadband amplified spontaneous emission (ASE) laser source is used as probe light to excite WGMs of the PMBR through taper fiber. Notably, the broadband laser source with a wide range spectral band (1528–1565 nm) can excite major resonant modes, providing abundant sensing information for high-precision measurement. In addition, the broadband laser source is low-cost, and do not require special optical bench, offering an opportunity to take WGM sensors out of the lab for engineering applications. A fiber polarization controller is used to achieve the optimal coupling efficiency by tuning the polarization state of the input light. In order to facilitate heating, the MBR and tapered fiber coupling system is packaged on a slide by using low-refractive-index polymer (MY-133, MY Polymers Ltd), which also enhances the coupling stability and avoids the interference of environmental contaminants, as displayed in Fig. 1(c). In addition, a polyimide electrothermal film is applied to heat PMBR, whose temperature is regulated via a computer-controlled thermoelectric cooler. Meanwhile, a thermistor is used to in-lined monitor and calibrate the temperature. The optical spectrum analyzer with the accuracy of 0.02 nm and sampling interval of 0.005 nm is employed to monitor and collect transmission spectra at different temperatures to provide the raw data for subsequent machine learning.

The typical quality (Q)-factor of PMBR is about 1.55×10^4 via Lorentzian fitting of the transmission spectrum, as displayed in Fig. 1(d). Remarkably, the multimode sensing method can still exhibit good sensing performance despite the low Q-factor. And the cross-application with machine learning can further achieve high detection accuracy. Furthermore, the long-term stability of wavelength shift and transmittance is demonstrated in Fig. 1(e). The drift deviations for wavelength and transmittance are 0.303 and 9.393×10^{-4}, respectively. The inset of Fig. 1(e) illustrates the calculated Allan variance, reflecting the noise level of the measurement system. It is observed that the Allan variance of wavelength shift reaches the least value at around 8 s, and the stabilization time of the wavelength is significantly affected by thermal effects, as shown in the left of the inset of Fig. 1(e). In addition, the Allan variance of the transmittance decreases by orders of magnitude and remains clearly visible for up to 32 s, as shown in the right of the inset of Fig. 1(e). Fig, 2(a) shows the typical transmission spectrum when the temperature is 26 °C, exhibiting the dense spectral characteristics of PMBR. Fig. 2(b) exhibits the evolution of the typical transmission spectrum with the resonant wavelength near 1553.6 nm as the temperature increases from 25.5 °C to 30.5 °C in steps of 0.5 °C. It is obvious that the resonance wavelength gradually blueshifts with increasing temperature, which is mainly attributed to the negative thermo-optic response of the polymer. The measurement temperature sensitivity of 21.6 pm/°C is obtained by linearly fitting the resonant wavelength changes, as shown in Fig. 2(c). Applying one-tenth of the linewidth (11 pm) is the uncertainty of the measurement system [32], and the detection limit of the single-mode sensing method is 0.509 °C.

Machine learning-assisted multimode sensing

A three-layer perceptron neural network is employed for the multimode sensing information fusion, while the transmission spectra are collected to establish database for training and testing the model, as shown in Fig. 3(a). Here, the training and testing spectrum in database are random arranged. Firstly, each input spectrum in Fig. 3(a) is normalized, and then converted into a matrix with one row and n columns, thus a matrix of m rows and n columns is formed when m spectra are input, as shown in Fig. 3(b). Next, the training and testing datasets with corresponding temperature labels are input into the fully connected three-layer perceptron neural network to estimate the target temperature and verify overall performance, as displayed in Fig. 3(c).

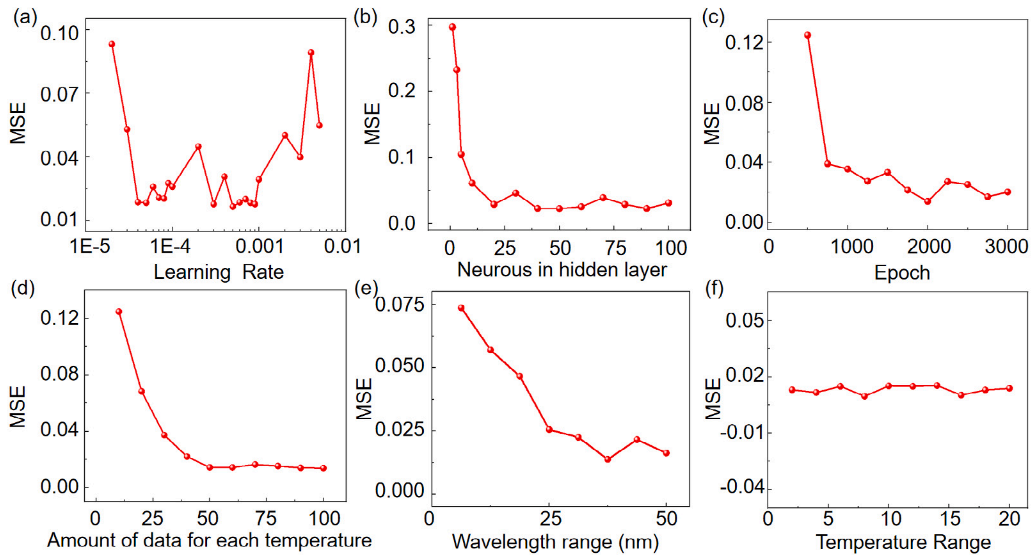

Fig. 4. MSE versus (a) learning rate, (b) neurons' number in hidden layer, (c) epochs, (d) dataset size, (e) wavelength range, and (f) temperature range.

When the transmission spectra are fed into the network, the input layer receives the complete raw data and transfers it to the hidden layer, and then passes it to the output layer to output predict temperature.

$$y = \sum_{i=1}^{k} w_i F\left(w_0 + \sum_{j=1}^{n} x_i w_{ij} \right) \tag{1}$$

where w_i is the weight factor of the input layer of the link, $F()$ is the nonlinear activation function, w_0 is the bias, x_i is the input data and $w_{i,j}$ is the weight factor of the output layer of the link.

Experimentally, the raw spectral data are collected when the temperature changes from 25 °C to 45 °C with the step of 0.5 °C. There are 80 groups of transmission at each temperature for training the neural network while 20 groups of transmission spectra are collected for blinding test, resulting in a total of 3280 training samples and 820 testing samples to form a database, as shown in Fig. 3(a). Here, each spectrum in the dataset is labeled with the corresponding temperature. Remarkably, the good stability of the measurement system allows the network model to achieve high accuracy predictions even with small samples. Subsequently, the neural network is trained using the back-propagation algorithm, which is based on the gradient descent method to adjust the weights [37]. After completing the training process, the nonlinear mapping relationship between the transmission spectrum and the corresponding temperature is established in the MLP neural network. Finally, the transmission spectrum of testing datasets is inputted into the trained MLP neural network, then the target temperature will be directly readout. The nonlinear activation function is set as Rectified Linear Unit (ReLU). The prediction of each temperature takes only 3 ms on the CPU of the AMD Ryzen 3750H 2.30 GHz, enabling the in-situ real-time monitoring of the PMBR-based temperature sensor. The loss function is defined as MSE to evaluate the performance of the neural network model, which can be expressed as:

$$MSE = \frac{1}{K} \sum_{i=1}^{K} (T_k - \hat{T}_k)^2 \tag{2}$$

where T_k is the true value of temperature and $\hat{T}_k$ is the predicted value of temperature.

In order to optimize the training hyper-parameters, we investigate the relationship between the learning rate and neurons' number of hidden layers and the MSE, as shown in Fig. 4(a)–(b). The MSE is minimized when the learning rate is set to 0.0005 and the number of neurons in the hidden layer is set to 50. Fig. 4(c) shows the effect of epoch on MSE, indicating that MSE gradually decreases as epoch increases and reaches the lowest value at 2000 epochs. Therefore, the hyper-parameters with optimal performance (i.e. the lowest MSE) come from the combination of a learning rate of 0.0005, 50 neurons of the hidden layer, and 2000 epochs. In addition to the neural network parameters, the amount of data used also affects the measurement results. Fig. 4(d) interrogates the effects of the total amount of data on MSE for each temperature. The larger data volume tends to result in a smaller MSE, while also reducing the impact of data randomness. In addition, to evaluate the performance of multimode sensing methods, we investigate the influences of wavelength range on MSE, as shown in Fig. 4(e). It is observed that the larger wavelength range means the lower MSE and the MSE reaches the best results when the wavelength range is 37.5 nm. This is mainly because this range contains the complete spectral data and provides the maximum amount of sensing information. Fig. 4(f) demonstrates the effect of temperature range on MSE. The temperature range starts at 25 °C and the step size is 0.5 °C. All of the MSEs are less than 0.02, indicating that this method has good generalization in terms of measurement range.

Furthermore, the predicted temperature for all testing datasets against the actual temperature is interrogated. The coefficient of determination ($R^2 = 1 - \sum(T - \hat{T})^2 / (T - \overline{T})^2$) is introduced to characterize the temperature retrieval performance of the models, where T is the standard actual value, $\hat{T}$ is the predicted value, $\overline{T}$ is the mean of actual value. Fig. 5(a) displays that the predicted temperature exhibits a good linear relationship with the actual temperature. The prediction capability of temperature has reached a high value of $R^2 = 0.9996$. It is observed that each prediction point falls near the true value, and even the temperature at both ends can be accurately predicted. In addition, the prediction error distribution is plotted in Fig. 5(b). Over 90% of the predicted temperature errors are less than 0.20 °C and 97.4% of the predicted temperature errors are less than 0.25 °C, which verifies the high accuracy of the measuring temperature method proposed in this paper. Finally, by comparing the predicted temperature with the actual temperature, it is concluded that the MSE is 0.0138, and the lower limit of detection (LOD) is 0.117 °C (approximated as the root mean square error, RMSE), which is three times lower than single-mode sensing methods, suggesting the excellent performance of multimode sensing method. As displayed in Fig. 4, the LOD can be improved by increasing the data size, neurons of hidden layer, and wavelength range. In addition, by introducing the physical mechanism to provide prior physical information for machine learning model, the reliability and interpretability of the model can be further enhanced, and thus improving the LOD.

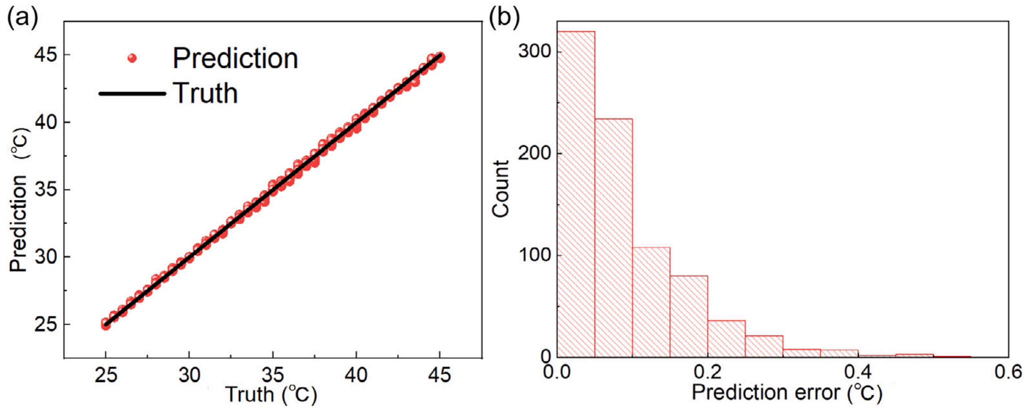

Fig. 5. (a) Comparison of predicted and true values of temperature. (b) Histogram of the error distribution of (a).

Conclusion

In summary, based on a low-cost broadband laser source, we reported a machine learning-assisted high-precision WGM temperature sensors by combining multimode sensing method. The raw data is consisted of a large number of multimode spectra and corresponding temperatures, which are analyzed and predicted using a MLP neural network. The actual temperatures are precisely measured with MSE of 0.0138. By fitting the predictions and standard temperature, the coefficient of determination R^2 of 0.9996 is achieved, demonstrating the excellent performance of MLP on temperature retrieval. The proposed multimode mode sensing method realizes a lower detection limit of 0.117 °C, which is lower three times than single-mode sensing methods. This work exhibits the potential for high-precision intelligent temperature sensors based on WGM microcavity, while providing a new thought for the practicability of optical microcavity sensors.

CRediT authorship contribution statement

Rui Song: Writing – original draft, Visualization, Software, Methodology, Investigation, Data curation. **Xuan Zhang:** Writing – review & editing, Validation, Supervision, Project administration, Investigation. **Shuang Feng:** Software, Investigation, Data curation. **Songyi Liu:** Validation, Methodology, Investigation. **Bing Duan:** Writing – review & editing, Validation, Supervision, Investigation. **Daquan Yang:** Writing – review & editing, Project administration, Funding acquisition.

Declaration of competing interest

The authors declare that they have no known competing financial interests or personal relationships that could have appeared to influence the work reported in this paper.

Data availability

Data will be made available on request.

Acknowledgments

This work was supported by National Key R&D Program, China (SQ2023YFB2805600); Beijing Nova Program from Beijing Municipal Science and Technology Commission, China (20230484433); Fundamental Research Funds for the Central Universities, China (2023PY08); State Key Laboratory of Information Photonics and Optical Communications, China (IPOC2021ZT01), BUPT, China; and BUPT Innovation and Entrepreneurship Support Program, China (2024-YC-T006).

References

[1] Vahala KJ. Nature 2003;424(6950):839–46.
[2] Yu D, Humar M, Meserve K, Bailey RC, Chormaic SN, Vollmer F. Nat Rev Methods Primers 2021;1(1):83.
[3] Watanabe K, Wu H-Y, Xavier J, Joshi LT, Vollmer F. Small 2022;18(15):2107597.
[4] Zhi Y, Yu X-C, Gong Q, Yang L, Xiao Y-F. Adv Mater 2017;29(12):1604920.
[5] Kippenberg TJ, Gaeta AL, Lipson M, Gorodetsky ML. Science 2018;361(6402):eaan8083.
[6] Wan S, Niu R, Wang Z-Y, Peng J-L, Li M, Li J, et al. Photon Res 2020;8(8):1342–9.
[7] Liu J, Bo F, Chang L, Dong C-H, Ou X, Regan B, et al. Sci China Phys Mech Astron 2022;65(10):104201.
[8] Dong C, Wang Y, Wang H. Natl Sci Rev 2015;2(4):510–9.
[9] Wang Y, Zeng S, Humbert G, Ho H-P. Laser Photonics Rev 2020;14(12):2000135.
[10] Jiang X, Qavi AJ, Huang SH, Yang L. Matter 2020;3(2):371–92.
[11] Zhao X, Guo Z, Zhou Y, Guo J, Liu Z, Li Y, et al. Micromachines 2022;13(4):592.
[12] Yu X-C, Tang S-J, Liu W, Xu Y, Gong Q, Chen Y-L, et al. Proc Natl Acad Sci 2022;119(6):e2108678119.
[13] Peng Z-D, Yu C-Q, Ren H-L, Zou C-L, Guo G-C, Dong C-H. Opt Lett 2020;45(16):4440–3.
[14] Zhu J, Ozdemir SK, Xiao Y-F, Li L, He L, Chen D-R, et al. Nat Photon 2010;4(1):46–9.
[15] Li Z, Zhang H, Nguyen BTT, Luo S, Liu PY, Zou J, et al. Photon Res 2021;9(2):B38–44.
[16] Venketeswaran A, Lalam N, Wuenschell J, Ohodnicki Jr. PR, Badar M, Chen KP, et al. Adv Intell Syst 2022;4(1):2100067.
[17] Zhang Y, Lu J, Le Z, Dong C-H, Zheng H, Qin Y, et al. IEEE Photonics J 2021;13(2):1–11.
[18] Yang D-Q, Chen J-H, Cao Q-T, Duan B, Chen H-J, Yu X-C, et al. Light: Sci Appl 2021;10(1):128.
[19] Liao J, Yang L. Light: Sci Appl 2021;10(1):32.
[20] Wu Y, Duan B, Li C, Yang D. Front Optoelectron 2023;16(1):29.
[21] Wu Y-R, Duan B, Song J, Tian H-P, Chen J-H, Yang D-Q, et al. Opt Express 2023;31(12):18851–61.
[22] Chen Q, Chen L, Fu Z, Xie S, Lu Q, Zhang X. IEEE Sens J 2023.
[23] Mathew J, Schneller O, Polyzos D, Havermann D, Carter RM, MacPherson WN, et al. J Lightwave Technol 2015;33(12):2419–25.
[24] Johari MAM, Khudus MIMA, Jali MHB, Al Noman A, Harun SW. Sensors Actuators A 2018;284:286–91.
[25] Savchenkov AA, Matsko AB, Ilchenko VS, Yu N, Maleki L. J Opt Soc Am B 2007;24(12):2988–97.
[26] Smith DL, Nguyen LV, Ottaway DJ, Cabral TD, Fujiwara E, Cordeiro CM, et al. Opt Express 2022;30(7):10443–55.
[27] Naku W, Zhu C, Nambisan AK, Gerald RE, Huang J. Opt Express 2021;29(24):40000–14.
[28] Wang Z, Liu Y, Gong C, Yuan Z, Shen L, Chang P, et al. PhotoniX 2021;2(1):18.
[29] Qi Y, Liu Y, Luo J. PhotoniX 2023;4(1):22.
[30] Jing J, Liu K, Jiang J, Xu T, Xiao L, Zhan X, et al. Adv Sci 2023;10(15):2207437.
[31] Fang J, Swain A, Unni R, Zheng Y. Laser Photonics Rev 2021;15(2):2000422.
[32] Chen H, Wang Z, Wang Y, Yu C, Niu R, Zou C-L, et al. Opt Express 2023;31(10):16781–94.
[33] Duan B, Zou H, Chen J-H, Ma CH, Zhao X, Zheng X, et al. Photon Res 2022;10(10):2343–8.
[34] Lu J, Niu R, Wan S, Dong C-H, Le Z, Qin Y, et al. IEEE Sens J 2021;21(7):9046–53.
[35] Yang D, Duan B, Wang A, Pan Y, Wang C, Ji Y, et al. J Lightwave Technol 2020;38(16):4555–9.
[36] Yang D-Q, Wang A, Chen J-H, Yu X-C, Lan C, Ji Y, et al. Photon Res 2020;8(4):497–502.
[37] Lecun Y, Bengio Y, Hinton G. Nature 2015;521(7553):436–44.